Original Research

Caudate Nuclei Volume, Diffusion Tensor Metrics, and T_2 Relaxation in Healthy Adults and Relapsing-Remitting Multiple Sclerosis Patients: Implications for Understanding Gray Matter Degeneration

Khader M. Hasan, PhD,[1]* Christopher Halphen, BA,[1] Arash Kamali, MD,[1] Flavia M. Nelson, MD,[2] Jerry S. Wolinsky, MD,[2] and Ponnada A. Narayana, MD[1]

Purpose: To investigate the utility of caudate nuclei (CN) macro- and microstructural metrics as markers of gray matter degeneration in healthy adults and relapsing-remitting multiple sclerosis (RRMS) patients.

Materials and Methods: The normal age- and pathology-related changes in caudate nuclei volume (CNV), the corresponding diffusion tensor metrics, and the T_2 relaxation times were measured in a cohort of 32 healthy adults (12 men/20 women; age range 21–59 years) and 32 age-matched RRMS patients (8 men/34 women; age range 21–57 years).

Results: Smaller values in both the absolute CNV and the caudate volume ratio relative to the total intracranial volume (CNVp) were observed in the RRMS group relative to healthy controls. The fractional anisotropy (FA), based on the diffusion tensor imaging (DTI) of the CN increased with age in healthy adults ($r = 0.52$; $P = 0.003$) but not in patients ($r = 0.28$; $P = 0.12$). The caudate FA value was approximately 9% larger in RRMS patients relative to controls ($P = 0.001$). The mean diffusivity of the CN was greater in the RRMS group compared to controls ($P = 0.02$). The caudate T_2 relaxation times were smaller in the RRMS group relative to the control group (3% reduction, $P = 0.05$). T_2 relaxation times did not exhibit age-related changes ($P > 0.35$) in either cohort. Strong and significant correlations between CNVp and whole-brain lesion load ($r = -0.48$; $P = 0.005$) and whole-brain CSF fraction ($r = -0.46$; $P = 0.01$) were also noted.

Conclusion: These preliminary findings indicate that caudate DTI-derived metrics can serve as potential quantitative radiological markers of MS pathology.

Key Words: caudate nuclei; relapsing-remitting multiple sclerosis; diffusion tensor imaging; T_2 relaxation; natural aging
J. Magn. Reson. Imaging 2009;29:70–77.

THE CAUDATE NUCLEI (CN), part of the basal ganglia, are involved in fine motor and cognitive functions (1). The caudate volume depends on a number of factors that include the neuropil (neurons and glia), extracellular space, dendrite proliferation, and connections (2,3). CN atrophy has been used as a marker of brain gray matter loss in natural aging (4) and in several neurological disorders (4,5).

The volume (6,7) and perfusion (8) of the CN have been reported to be significantly smaller in multiple sclerosis (MS) patients compared to age-matched healthy controls. Caudate atrophy has been associated with disability, as assessed by the extended disability status score (EDSS) in MS (7,9,10). Caudate atrophy appears to be related to lesion load (11) and fatigue (12) in MS. Caudate signal abnormalities on MRI have been related to cognitive deficit (13) and to emotional dysfunction or "abulia" (14).

The exact mechanisms responsible for caudate volume changes in healthy aging and its complex interplay with pathology in MS have yet to be explored. The availability of noninvasive and quantitative neuroimaging markers might provide useful clues about the neuronal substrates of neurodegeneration in MS.

In this study, the entire CN "macrostructural" volumes and the corresponding "microstructural" metrics derived from diffusion tensor imaging (DTI) and T_2 relaxation times were determined in age- and gender-matched cohorts of healthy controls and relapsing-remitting MS (RRMS) patients to investigate the interplay among caudate volume loss, disease duration (DD), and

[1]Department of Diagnostic and Interventional Imaging, University of Texas Health Science Center at Houston, Houston, Texas, USA.
[2]Department of Neurology, University of Texas Health Science Center at Houston, Houston, Texas, USA.
Contract grant sponsor: American National Institutes of Health; Contract grant numbers: NIH/NINDS R01-NS052505–03; NIH/NIBIB EB002095.
Presented in abstract form at the 16th Annual Meeting of ISMRM, Toronto, Ontario, Canada, 2008.
*Address reprint requests to: K.M.H., 6431 Fannin St., MSB 2.100, Houston, TX 77030. E-mail: Khader.M.Hasan@uth.tmc.edu
Received August 14, 2008; Accepted October 8, 2008.
DOI 10.1002/jmri.21648
Published online in Wiley InterScience (www.interscience.wiley.com).

Table 1
Basic Demographics and MRI Information on the Healthy Adult Group Brains

Healthy controls	Men	Women	Men and women	Men vs. women (*P*)
Number of subjects	12	20	32	0.16
Age (years)[a]	37.4 ± 11.6, [24.2–57.6], 33.3	38.2 ± 11.5, [21.7–58.6], 39.2	38.7 ± 11.5, [21.7–58.6], 35.9	0.75
ICV (mL)	1598.2 ± 147.2	1484.7 15.6	1527.3 ± 137.8	0.02
CNV (mL)	7.49 ± 0.86	7.00 ± 0.79	7.18 ± 0.84	0.11
CNVp	0.470 ± 0.047	0.472 ± 0.039	0.471 ± 0.041	0.88
WBCSFp	10.58 ± 2.48	9.76 ± 2.97	10.01 ± 2.78	0.43

[a]Values are mean ± SD, range [minimum-maximum], and median.
CNV = caudate nuclei volume in mL (1 mL = 1 cm^3), CNVp = caudate nuclei volume to intracranial volume percentage (CNV/ICV*100%), ICV = intracranial volume (in mL = cm^3), WBCSFp = whole brain cerebrospinal fluid to intracranial volume percentage (CSFv/ICV*100%).

disability in relation to normal aging, global lesion load, and brain atrophy.

MATERIALS AND METHODS

Study Population

This MRI protocol was approved by our institutional review board (IRB). Healthy adult controls (N = 32; mean age ± SD = 38.7 ± 11.5 years; Table 1) were recruited from the local community and university staff. All healthy subjects were screened for history of trauma, surgery, chronic illness, alcohol and/or drug abuse, neurological illness, and current pregnancy. Controls in this study did not report any neurological conditions and the MR images were judged to be normal. The patient demographics are summarized in Table 2. The EDSS was assessed as described by Kurtzke (15). All but nine of the RRMS patients were on first-line immunomodulatory therapies. All but one was clinically stable for more than one year without relapses prior to the MRI session. Written informed consent was obtained from each subject.

MRI Data Acquisition

All MRI studies were performed on a 3T Philips Intera scanner with a dual quasar gradient system with a maximum gradient amplitude of 80 mT/m and an eight-channel sensitivity encoding (SENSE)-compatible head coil (Philips Medical Systems, Best, The Netherlands).

Conventional MRI

The MRI protocol included: 1) dual fast spin echo (FSE) with echo (TE) and repetition (TR) times of $TE_1/TE_2/TR$ = 8.2/90/6800 msec, 2) fluid-attenuated inversion recovery (FLAIR; $TE/T_I/TR$ = 80/2500/80 msec), and 3) fast dual inversion recovery (DIR; $TE/T_{I1}/T_{I2}/TR$ = 32/325/3400/15000 msec) sequence (16) for suppressing cerebrospinal fluid (CSF) and white matter. The slice thickness for both conventional and diffusion-weighted images was 3.0 mm with 44 contiguous axial slices covering the entire brain and a square field of view (FOV) of 240 mm × 240 mm (i.e., voxel dimensions = 0.9375 mm × 0.9375 mm × 3.0 mm).

DTI Data Acquisition

The DTI data were acquired using a single-shot, spin-echo, diffusion-sensitized, echo-planar imaging sequence with a balanced Icosa21 tensor encoding scheme (i.e., 21 uniformly distributed directions over the unit hemisphere) (17), b-factor = 1000 seconds mm^{-2}, TR/TE = 7100/65 msec. The number of b ~ 0 magnitude image averages was six. In addition, each diffusion encoding was repeated twice and magnitude-averaged to enhance the signal-to-noise ratio (SNR).

Table 2
Demographic, Clinical, and Imaging Data of the RRMS Patients

RRMS patients	Men	Women	Men and women	Men vs. women (*P*)
Number of patients	8	24	32	0.005 (χ^2-test)
Age (years)[a]	40.9 ± 8.5, [25.6–50.1], 41.8	42.2 ± 8.6, [21.9–56.6], 43.7	41.9 ± 8.5, [21.9–56.6], 43.3	0.72 (*t*-test)
DD (years)[a]	5.8 ± 7.2, [0.2–22.3], 2.5	9.8 ± 8.0, [0.4–30.3], 8.8	9.0 ± 9.0, [0.2–30.3], 6.3	0.22 (*t*-test)
EDSS[a]	1.5 ± 1.0, [0.0–3.0], 1.75	1.7 ± 1.6, [0.0–6.5], 1.75	1.7 ± 1.5, [0.0–6.5], 1.75	0.46 (Mann-Whitney)
Lesion volume (mL)[a]	11.7 ± 15.9, [0–47.2], 5.1	14.6 ± [1.3–41.6], 12.3	10.9 ± 116, [0.0–47.2], 9.8	0.61 (*t*-test)
ICV (mL)	1562.0 ± 140.9	1453.8 ± 120.6	1480.9 ± 132.5	0.04 (*t*-test)
CNV (mL)	6.54 ± 1.14	5.95 ± 0.94	6.1 ± 1.00	0.15 (*t*-test)
CNVp	0.422 ± 0.085	0.412 ± 0.076	0.415 ± 0.077	0.75 (*t*-test)
WBCSFp	12.5 ± 3.6	13.9 ± 4.1	13.6 ± 4.0	0.38 (*t*-test)
WBLVp[a]	0.78 ± 1.03, [0.0–3.0], 0.30	1.0 ± 0.90 [0.1–2.9], 0.80	0.93 ± 0.95, [0.0–3.0], 0.65	0.57 (*t*-test)

[a]Values are mean ± SD, range [minimum–maximum], and median.
DD = disease duration; EDSS = expanded disability status score; RRMS= relapsing and remitting multiple sclerosis; CNVp = caudate nuclei volume to intracranial volume percentage (CNV/ICV*100%), WBLVp = whole brain lesion volume percentage (LV/ICV*100%); WBCSFp = whole brain cerebrospinal fluid to intracranial volume percentage (CSFv/ICV*100%).

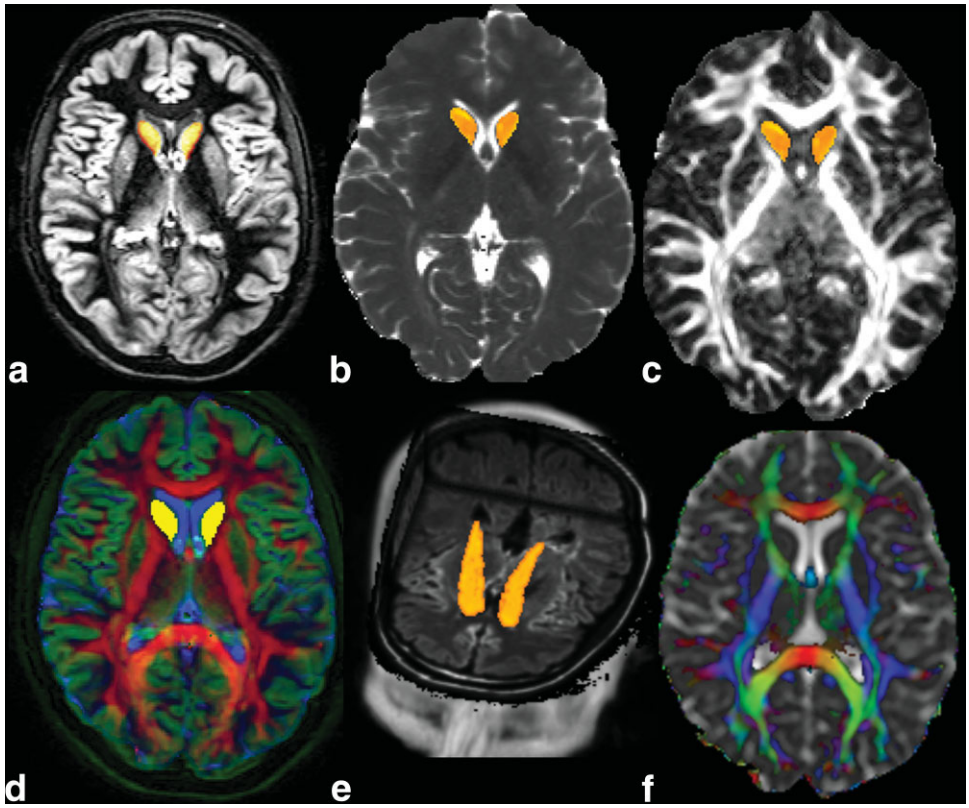

Figure 1. Illustration of the CNV delineation, conventional, and DT-MRI data fusion using the data obtained from one RRMS patient: (**a**) DIR (white matter and CSF suppressed) or gray matter-only map (DIR-GM), (**b**) T_2 relaxation time map, (**c**) FA map, (**d**) an image fusion along the three red-green-blue channels (RGB) of {FA, DIR-GM, T_2} maps, (**e**) a three-dimensional view of the caudate with the FLAIR volume in the background, and (**f**) the principal DT eigenvector modulated with FA and fused with the mean diffusivity (red indicates right–left connections [commissural pathways], green indicates anterior–posterior connections [association pathways], and blue represents inferior–superior connections [projection pathways]). Note that in (d), FA highlights white matter (red), DIR highlights gray matter (green), and T_2 highlights CSF (blue). The axial two-dimensional representative sections in (a–c), (e), and (f) are obtained at the level of the lateral ventricles and show the caudate head only; the three-dimensional view in (e) shows the head and body of the caudate on the FLAIR background.

The total DTI acquisition time was less than seven minutes (4).

DTI and Conventional MRI Data Processing

Diffusion-weighted images were intraregistered to the baseline "b_0" images (without diffusion weighting) to correct for the eddy-current-induced image distortions using the software on the Philips PRIDE workstation (Philips Medical Systems, Best, The Netherlands). Next, the DIR and FSE image volumes were coaligned with the b_0 reference volumes using the mutual information based coregistration in SPM (http://www.fil.ion.ucl.ac.uk/spm/software/spm2). The T_2 values were estimated from the early (TE_1) and late echo (TE_2) images according to standard spin-echo procedures assuming a single compartment model (4). The T_2, fractional anisotropy (FA), and mean diffusivity (D_{av}) values were saved for further analysis.

CNV Delineation

Using MRIcro (http://www.sph.sc.edu/comd/rorden/mricro.html), the CN were manually traced by a trained rater on eight to 10 consecutive slices on the axial DIR images to create a mask for volumetry and DT analysis using a validated procedure described elsewhere (4). The CN delineation followed anatomical landmarks as detailed elsewhere (4). Accuracy of the caudate manual tracing was verified by overlaying the FA and D_{av} maps on the caudate mask (Fig. 1). All data sets were masked to remove nonbrain tissues to estimate the intracranial volume (ICV) for each subject for normalization (4). To reduce the number of comparisons, the volume of the entire caudate (right and left hemispheres) was estimated since published reports on the caudate volume in healthy adult controls show no statistically significant gender dependence or laterality in the caudate volume (4–7,18).

Lesion Load Segmentation Using Conventional MRI

Brain images were segmented into white matter, gray matter, CSF, and lesions using the coregistered multispectral dual FSE and the FLAIR image volumes as described elsewhere (19). The lesion volume (LV) and CSF percentages in the whole brain (WB) were normalized to account for the intersubject variability (i.e.,

Table 3
Comparison Between Controls and RRMS Age and Group Means of Various MRI-Derived Parameters of the Entire Caudate (Fractional Anisotropy, Mean Diffusivity, and T_2 Relaxation Time) Along With the Age Linear Regression and Correlation Statistical Analysis

	Healthy adult controls	RRMS	*P*
Age (years)	38.2 ± 11.4	41.9 ± 8.5	0.15
ICV (mL = cm^3)	1527.3 ± 137.8	1480.9 ± 132.5	0.17
WBCSFp	10.1 ± 2.8	13.6 ± 4.0	0.0001
CNV (mL)	7.18 ± 0.84	6.1 ± 1.01	0.000016
CNV_p = CNV/ICV (×100%)	0.47 ± 0.04;	0.41 ± 0.08;	0.0006;
$r_{age}(p)$	–0.38 (0.03)	–0.29 (0.11)	0.70
FA @ CNV	0.139 ± 0.011;	0.152 ± 0.017;	0.001;
$r_{age}(p)$	0.52 (0.003)	0.28 (0.12)	0.28
D_{av} ($\times 10^{-3}$ mm^2 $second^{-1}$) @ CNV	0.736 ± 0.023	0.751 ± 0.031;	0.02;
$r_{age}(p)$	0.16 (0.38)	–0.32 (0.07)	0.06
T_2 (msec) @ CNV	91.8 ± 5.2	89.4 ± 4.9;	0.05;
$r_{age}(p)$	0.16 (0.37)	0.09 (0.61)	0.79

WBLVp = LV/ICV * 100%; WBCSFp = CSF/ICV * 100%), where ICV is the sum of white matter, gray matter, lesion, and CSF volumes.

Statistical Analysis

Correlations between age, caudate volume, lesion load, DD, T_2 values, and DTI-derived metrics were computed using the Pearson correlation coefficient. Correlations between EDSS and all other variables were computed using the Spearman coefficient. Statistical significance was considered at $P \leq 0.05$. Slopes and rates of change of MRI metrics with age were compared using the *r*- to *z*-Fisher transform (20). Comparisons between the group means and medians were performed using ANOVA (*t*-test) and the Mann-Whitney U-test. Caudate volume reproducibility (4) and DTI quality control measures (21) are described elsewhere. All statistical analyses were performed using MATLAB R12.1 Statistical Toolbox v 3.0 (The MathWorks Inc., Natick, MA, USA).

RESULTS

Demographics and Clinical Information

There were no significant age differences between men and women in either the control ($P = 0.75$; Table 1) or the RRMS ($P = 0.72$; Table 2) group. The control and RRMS cohorts were age-matched ($P = 0.15$; Table 3). The ratio of women in the control group (20/32 = 62.5%) was not statistically different from the ratio (24/32 = 75%) in the RRMS group ($P = 0.55$; χ^2 test). The percentage of women in our RRMS population is consistent with the reported preponderance of RRMS in women (Table 2).

Gender-Based Caudate and WB Volumetry

There were significant differences in the ICV between men and women in the healthy control ($P = 0.02$) and RRMS ($P = 0.04$) groups. The caudate volume to intracranial volume percentage (CNVp = CNV/ICV * 100%) did not differ between men and women in either group. Nor was the CSF volume as a percentage of intracranial contents different between men and women in either group. In the RRMS group, there were no significant differences in the EDSS, DD, and WB LV to ICV percentage (WBLVp = LV/ICV × 100%) between men and women (Tables 1 and 2). As these comparisons indicated no statistical differences in entire caudate volume, normalized caudate, or WB metrics between males and females in the two groups, the data from men and women in the two groups were pooled.

Caudate and WB Differences between Healthy Controls and RRMS

The ICV was similar between controls and RRMS ($P = 0.17$; Table 3). The CNVp (13% decrease, $P = 0.0006$) were significantly smaller in the RRMS group compared to the age-matched controls. The WB CSF fraction was significantly larger in the RRMS group (31% increase, $P = 0.0001$; Table 3).

Group Comparisons of Entire Caudate FA, Mean Diffusivity, and T_2

The caudate mean FA values (9% increase, $P = 0.001$; Table 3) and D_{av} (2% increase; $P = 0.02$) in the CN were larger in the RRMS patients compared to healthy subjects. However, the caudate T_2 relaxation times were shorter in the RRMS group (~3% decrease; $P = 0.05$; see Table 3).

Age-Dependence of Caudate Metrics in both RRMS and Healthy Controls

Figure 2 shows scatter plots and regression of (a) caudate volume-to-ICV percentage, (b) FA, (c) mean diffusivity, and (d) T_2 relaxation times of caudate as a function of age for both adult controls and RRMS patients (see also Table 3). A significant decrease in CNVp as a function of age in controls ($r = -0.38$; $P = 0.01$) and a trend in RRMS patients ($r = -0.29$; $P = 0.11$) was observed. The caudate T_2 relaxation time did not exhibit significant correlations with age in either controls or patients ($P > 0.37$; Table 3 and Fig. 2). There were no significant differences in the age-related rates of change of caudate metrics between healthy controls and RRMS ($P > 0.05$; see Table 3).

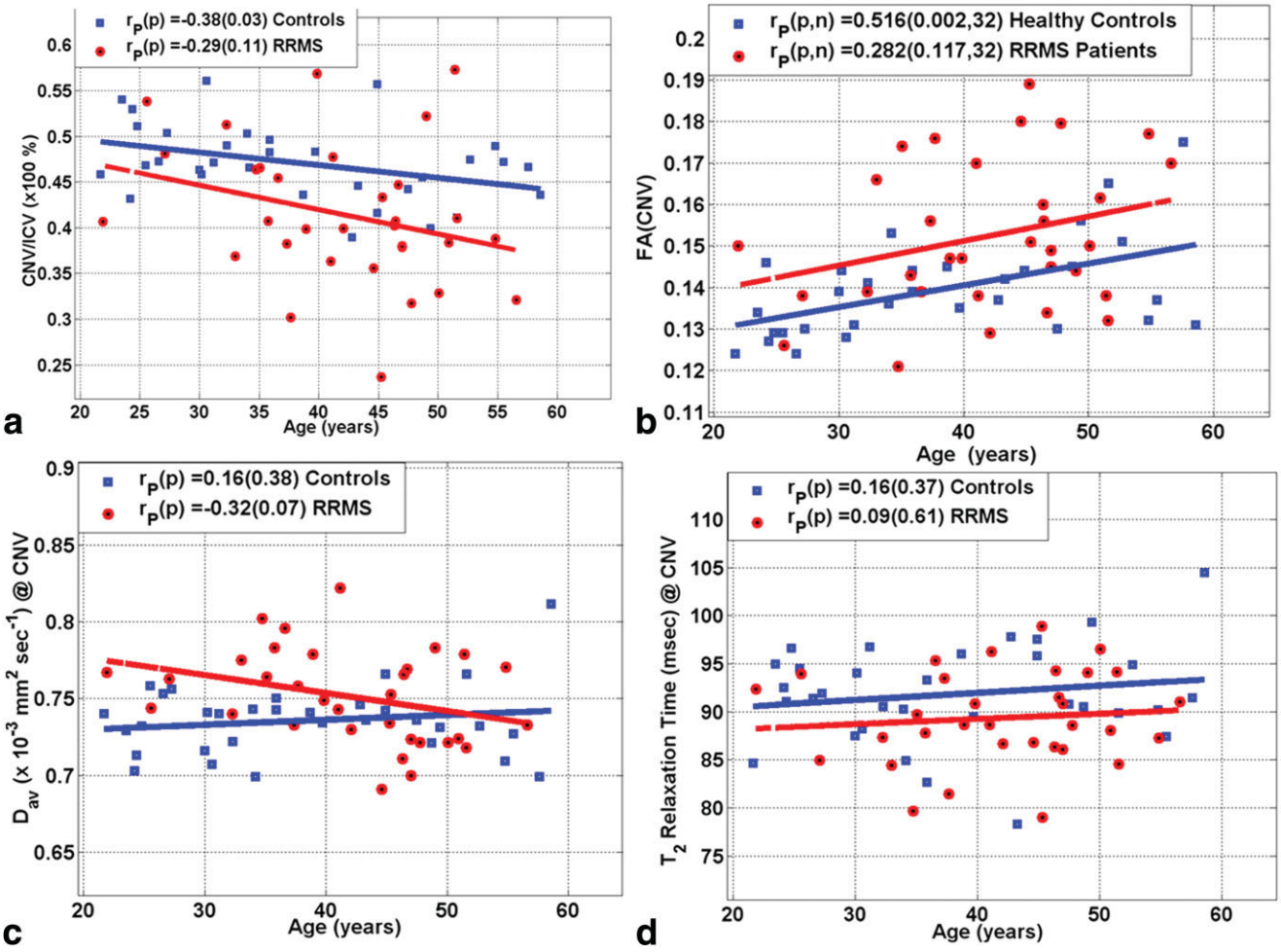

Figure 2. Scatter plots and regression analysis of the MRI metrics in the caudate of both healthy controls and RRMS patients as age advances: (**a**) CNVp = CNV/ICV*100%, (**b**) FA, (**c**) mean diffusivity, and (**d**) T_2 relaxation times. The group and correlations with age comparisons are summarized in Table 3. Note the decrease in CNVp, increase in FA, elevated mean diffusivity, and weak age dependence in both mean diffusivity and T_2 values. [Color figure can be viewed in the online issue, which is available at www.interscience.wiley.com.]

Correlation of Entire Caudate and Brain Atrophy With Clinical Scores in RRMS Patients

Table 4 summarizes the correlation coefficients and the corresponding *P*-values between demographic (age), clinical (DD and EDSS), and MRI-derived metrics of the CNVp, WBCSFp, and WBLVp. In the RRMS group, a strong correlation between the brain CSF fraction and caudate volume fraction is noted ($r = -0.457$; $P = 0.01$). The WBLVp correlated strongly with CNVp ($r = -0.482$; $P = 0.005$) and caudate mean FA ($r = 0.625$; $P = 0.0001$; Table 4).

Interplay Between Entire Caudate Micro- and Macrostructural Metrics

The scatter plots of CNVp and the corresponding FA(CN) (Fig. 3a) show an inverse linear relationship between the caudate volume fraction—a macrostructural index—and the corresponding FA—a microstructural index of tissue organization—in both healthy controls ({*r*(CNVp, FA)} = −0.38; $P = 0.04$) and RRMS patients ({*r*(CNVp, FA)} = −0.67; $P = 0.00002$; Table 4). Potentially useful relations between caudate metrics and WBCSFp on both controls are shown in the scatter plot of these two variables in Fig. 3b. Note the strong negative correlation in the RRMS group between CNVp and WBCSFp ($r = -0.46$; $P = 0.01$; Table 4). This direct association between CNVp and WBCSFp observed in the RRMS group was not seen in the age-matched healthy controls (Table 4; Fig. 3).

DISCUSSION

This is the first study on simultaneous measurement of the CNV in combination with the corresponding T_2 relaxation times and DTI metrics in age- and gender-matched adult controls and RRMS patients. We focused on normal-appearing CN to provide a simple objective and quantitative measure of deep gray matter atrophy in both healthy controls (4) and RRMS patients (6,7) using previously described and validated methodologies at high SNRs and optimal DT methods at 3.0T (4). In this work we adopted intrinsic MRI-derived metrics such as FA, D_{av}, T_2 relaxation time, and normalized

Table 4
Summary of Correlation Coefficient and Its Significance {r(p)} Between Demographic, Clinical, Whole Brain, and Caudate Nuclei Metrics on the RRMS Patient Group*

	DD	EDSS	WBLVp	WBCSFp	CNVp	FA(CN)	Dav(CN)	T2(CN)
Age	0.365	0.074	0.036	0.291	−0.291	0.296	−0.322	0.094
	(0.04)	(0.69)	(0.84)	(0.11)	(0.11)	(0.12)	(0.07)	(0.61)
DD	**1**	0.189	0.207	0.224	−0.24	0.296	−0.161	0.205
		(0.30)	(0.255)	(0.22)	(0.19)	(0.1)	(0.38)	(0.261)
EDSS		**1**	0.299	0.362	−0.143	0.078	0.311	0.311
			(0.097)	**(0.04)**	(0.43)	(0.67)	(0.08)	(0.084)
WBLVp			**1**	0.510	−0.482	0.625	−0.097	0.156
				(0.003)	**(0.005)**	**(0.0001)**	(0.60)	(0.40)
WBCSFp				**1**	−0.457	0.337	−0.089	0.122
					(0.01)	(0.06)	(0.63)	(0.51)
CNVp					**1**	−0.674	0.439	0.056
						(0.00002)	**(0.01)**	(0.76)
FA(CN)						**1**	−0.344	0.031
							(0.05)	(0.866)
D_{av}(CN)							**1**	0.119
								(0.52)

*Bold values correspond to statistically significant *P* values ($P \leq 0.05$). Examples to help read this table: r(DD,DD) = 1 ($P = 0$); Pearson r(age,DD) = r(DD,age) = 0.365 ($P = 0.04$); Spearman r(age,EDSS) = 0.074 ($P = 0.69$)}. The mean and SD values ($\mu \pm \sigma$) values for all variables on the RRMS patients are summarized in Table 2 and Table 3. The slope (β) for each variable (y) regressed against another variable (x) can be related to r: slope b = r * σ(y)/σ(x) (linear regression model: y = b * x + a + noise).

caudate volume after careful delineation and multimodal image registration.

These quantitative studies indicate a sex-independent caudate volume reduction in the RRMS patient group along with reduced T_2 relaxation times, elevated caudate FA, and increased mean diffusivity compared to the age-matched adult controls. Both control and RRMS subjects exhibited a negative correlation of caudate volume with age and a positive correlation between the caudate FA and age.

Sex, Age, and Diagnosis Effects on the CNV to Brain Percentage

Our results on the sex-independent loss of caudate volume and its fraction with age are consistent with several quantitative MRI studies on healthy controls (17,22,23) and some early postmortem studies on the caudate (3). Several previous studies have documented different aspects of caudate involvement in MS using measures such as caudate volume (6,7), normalized signal hypointensity (24), and region-of-interest (ROI) relaxation (14). Previous reports on the caudate in MS did not report age-related trends (6) and did not relate the dynamics of caudate volume changes to global measures of atrophy and lesion load. In our study we focused on one particular phenotype (RRMS) and explored the effect of covariates such as age, DD, lesion load, and global atrophy measures. Our work shows important sex-independent relations among caudate volume fraction, basic demographics, clinical scores, and WB atrophy measures (Figs. 2 and 3, Table 4).

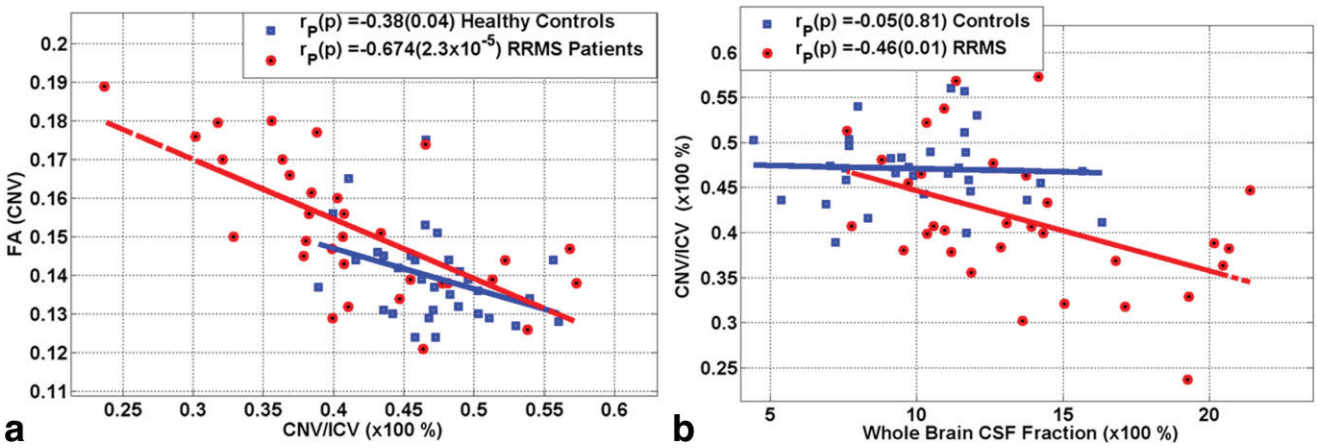

Figure 3. Representative scatter plots and regression analysis on both RRMS patients and controls of the interplay between (**a**) CNVp vs. FA (CN) and (**b**) WB CSF fraction vs. caudate to ICV fraction. Note the strong relationship between CNVp and caudate FA and WB CSF fraction (see also Tables 1–4). [Color figure can be viewed in the online issue, which is available at www.interscience.wiley.com.]

The caudate volume decrease with age reflects a general trend of atrophy of deep and cortical gray matter in healthy controls (22). The loss of deep and cortical gray matter in MS patients has been the focus of several studies (25).

Sex, Age, and Diagnosis Effects on the Caudate T_2 Relaxation Times

Our T_2 relaxation time measurements in the caudate in controls are consistent with an earlier ROI-based study by Agartz et al (26). The caudate mean diffusivity and T_2 relaxation values did not exhibit significant age-related trends in our adult population, suggesting minimal CSF contamination and uniform SNR (4).

The mean caudate T_2 relaxation times were smaller in the RRMS patients compared to healthy controls ($P = 0.05$; Table 3). This decrease in T_2 values is consistent with several previous MRI studies (13,24) that reported decreases in signal intensity, which have been hypothesized to be associated with iron accumulation (27). The iron-accumulation hypothesis for the interpretation of signal attenuation in the basal ganglia has been discussed in several reports (28).

Our data indicate that the caudate T_2-relaxation values in the RRMS did not increase with age (see Tables 3 4). A previous study using ROI T_1 relaxation measurements in the caudate of MS reported elevated values (14). The accumulation of iron in the caudate would have reduced both T_1 and T_2 relaxation times (29).

The T_2 values in a largely unmyelinated and homogeneous region such as the caudate are affected generally by countering the effects of increased cellular water, which tends to increase T_2 and the presence of free radicals (14), including paramagnetic iron (30), and reduce T_2 relaxation time (29,31). These two opposing effects reduce the apparent T_2 sensitivity to aging in young and middle-aged adults (21–59 years). However, this may be offset in older adults, where iron, for example, may accumulate due to altered recycling (31).

Sex, Age, and Diagnosis Effects on the Caudate DTI Metrics

A major finding in these studies is the reduced caudate volume, along with reduced T_2 relaxation times and elevated FA and mean diffusivity in the RRMS group. The caudate FA increased with age at comparable rates in both healthy adults and RRMS patients (Fig. 1, Table 3).

A comprehensive biophysical interpretation of in vivo DTI measurements in the human brain is not yet available (32). However, a slight increase in FA of the CN in healthy young and middle-aged men and women may be the result of neuronal and dendrite elimination with age resulting in reduced barriers to diffusion in an otherwise incoherent but specialized dendrite arbor (32). Targeted loss of certain dendrite connections would increase the anisotropy in gray matter, as has been summarized elsewhere (4). An excessive growth and disorganized arborization of dendrites may increase caudate volume and reduce anisotropy, as has been reported in children with fragile-X syndrome (33).

The dendrite-connection hypothesis of normal aging is also supported by histology (34). Targeted dendrite elimination in the caudate has been previously reported in demented Alzheimer's (34), Parkinson's (28), and Huntington's disease patients (35). Targeted elimination of dendrite arborization in the cortex (36) and thalamic-basal ganglia-cortical connections (37) has also been reported in MS.

Elevated diffusion anisotropy in the basal ganglia of patient populations compared to age-matched controls was recently observed in the basal ganglia of patients with Huntington's disease (38) or with spina bifida (39). A paradoxical increase in normal-appearing basal ganglia (caudate and putamen) DT anisotropy along with a reduction in the mean diffusivity was reported in the normal-appearing basal ganglia of MS patients by Ciccarelli et al (40). The authors excluded gliosis, which would have resulted in more disorganization (e.g., reduced anisotropy and increased T_2) and attributed this finding to axonal degeneration due to fiber transection in remote focal MS lesions (40).

Our preliminary studies may warrant further cross-sectional and longitudinal studies stratified by age, DD, and EDSS in larger normal and MS cohorts. The implication and correlation of the caudate volume loss and reduction in T_2 relaxation times to specific connected white matter fiber pathways, and the examination of regional distribution of lesions in MS are beyond the scope of this work and will be pursued in a future study.

A future extension of the current study is to examine whether these measurable changes in the caudate metrics are detectable early and have predictive value for the future course of the disease. Also, these are cross-sectional studies on a small RRMS population suggesting that the changes may well be dynamic and useful as a biomarker of change over time, but the sensitivity of this set of metrics to change over relatively short intervals (one to three years as in clinical trials) and the ability to detect therapeutic effects using these measures in clinical trials will require additional longitudinal studies that are beyond the scope of the current work.

In conclusion, we report simultaneous measurements of the human CNV along with water molecular DTI metrics and T_2 relaxation times in a cohort of healthy adults and RRMS patients. This study demonstrates that the CNV and the volume ratio relative to the ICV decreased with age in both men and women in the healthy and RRMS groups. The caudate FA increased with age and was larger in RRMS patients compared to controls, while T_2 relaxation times and mean diffusivity did not change with age. Both mean diffusivity and FA were elevated while T_2 was reduced in the RRMS compared to the age-matched adult controls. The age-dependent changes in caudate volume, DTI metrics, and the corresponding T_2 relaxation times may provide important noninvasive quantitative radiological markers to study the complex neuronal substrates that intertwine natural aging and neurodegenerative disease.

ACKNOWLEDGMENTS

We thank Vipul Kumar Patel for helping in the data acquisition. This work was funded by the American National Institutes of Health (NIH/NINDS R01-NS052505–03 (to K.M.H.) and NIH/NIBIB EB002095 (to P.A.N.).

REFERENCES

1. Alexander GE, de Long M, Strick PL. Parallel organization of functionally segregated circuits linking basal ganglia and cortex. Ann Rev Neurosci 1989;9:357–381.
2. Masliah E, Mallory M, Hansen L, DeTeresa R, Terry RD. Quantitative synaptic alterations in the human neocortex during normal aging. Neurology 1993;43:192–197.
3. Eggers R, Knebel G, Haug H. Morphometric studies of biological changes in synapses of the human caudate nucleus. Z Gerontol 1991;24:302–305.
4. Hasan KM, Halphen C, Boska MD, Narayana PA. Diffusion tensor metrics, T2 relaxation, and volumetry of the naturally aging human caudate nuclei in healthy young and middle-aged adults: possible implications for the neurobiology of human brain aging and disease. Magn Reson Med 2008;59:7–13.
5. Mascalchi M, Lolli F, Della Nave R, et al. Huntington disease: volumetric, diffusion-weighted, and magnetization transfer MR imaging of brain. Radiology 2004;232:867–873.
6. Bermel RA, Innus MD, Tjoa CW, Bakshi R. Selective caudate atrophy in multiple sclerosis: a 3D MRI parcellation study. Neuroreport 2003;14:335–339.
7. Sharma J, Sanfilipo MP, Benedict RH, Weinstock-Guttman B, Munschauer 3rd FE, Bakshi R. Whole-brain atrophy in multiple sclerosis measured by automated versus semiautomated MR imaging segmentation. AJNR Am J Neuroradiol 2004;25:985–896.
8. Inglese M, Park SJ, Johnson G, et al. Deep gray matter perfusion in multiple sclerosis: dynamic susceptibility contrast perfusion magnetic resonance imaging at 3 T. Arch Neurol 2007;64:196–202.
9. Caon C, Zvartau-Hind M, Ching W, Lisak RP, Tselis AC, Khan OA. Intercaudate nucleus ratio as a linear measure of brain atrophy in multiple sclerosis. Neurology 2003;60:323–325.
10. Zhang Y, Zabad RK, Wei X, Metz LM, Hill MD, Mitchell JR. Deep grey matter "black T2" on 3 Tesla magnetic resonance imaging correlates with disability in multiple sclerosis. Mult Scler 2007;13: 880–883.
11. Prinster A, Quarantelli M, Orefice G, et al. Grey matter loss in relapsing-remitting multiple sclerosis: a voxel-based morphometry study. Neuroimage 2006;29: 859–867.
12. Roelcke U, Kappos L, Lechner-Scott J, et al. Reduced glucose metabolism in the frontal cortex and basal ganglia of multiple sclerosis patients with fatigue: a 18F-fluorodeoxyglucose positron emission tomography study. Neurology 1997;48:1566–1571.
13. Brass SD, Benedict RH, Weinstock-Guttman B, Munschauer F, Bakshi R. Cognitive impairment is associated with subcortical magnetic resonance imaging grey matter T2 hypointensity in multiple sclerosis. Mult Scler 2006;12:437–444.
14. Niepel G, Tench ChR, Morgan PS, Evangelou N, Auer DP, Constantinescu CS. Deep gray matter and fatigue in MS: a T1 relaxation time study. J Neurol 2006;253:896–902.
15. Kurtzke JF. Rating neurologic impairment in multiple sclerosis: an expanded disability status scale (EDSS). Neurology 1983;33:1444–1452.
16. Bedell BJ, Narayana PA. Implementation and evaluation of a new pulse sequence for rapid acquisition of double inversion recovery images for simultaneous suppression of white matter and CSF. J Magn Reson Imaging 1998;8:544–547.
17. Hasan KM, Narayana PA. Computation of the fractional anisotropy and mean diffusivity maps without tensor decoding and diagonalization: theoretical analysis and validation. Magn Reson Med 2003; 50:589–598.
18. Krishnan KR, Husain MM, McDonald WM, et al. In vivo stereological assessment of caudate volume in man: effect of normal aging. Life Sci 1990;47:1325–1329.
19. Sajja BR, Datta S, He R, et al. Unified approach for multiple sclerosis lesion segmentation on brain MRI. Ann Biomed Eng 2006;34: 142–151.
20. Glantz SA. Primer of biostatistics. 5th ed. New York: McGraw-Hill; 2002.
21. Hasan KM. A framework for quality control and parameter optimization in diffusion tensor imaging: theoretical analysis and validation. Magn Reson Imaging 2007;25:1196–1202.
22. Walhovd KB, Fjell AM, Reinvang I, et al. Effects of age on volumes of cortex, white matter and subcortical structures. Neurobiol Aging 2005;26:1261–1270.
23. Ifthikharuddin SF, Shrier DA, Numaguchi Y, et al. 2000. MR volumetric analysis of the human basal ganglia: normative data. Acad Radiol 2000;7:627–634.
24. Bakshi R, Benedict RH, Bermel RA, et al. T2 hypointensity in the deep gray matter of patients with multiple sclerosis: a quantitative magnetic resonance imaging study. Arch Neurol 2002;59:62–68.
25. Charil A, Dagher A, Lerch JP, Zijdenbos AP, Worsley KJ, Evans AC. Focal cortical atrophy in multiple sclerosis: relation to lesion load and disability. Neuroimage 2007;34:509–517.
26. Agartz I, Saaf J, Wahlund LO, Wetterberg L. T1 and T2 relaxation time estimates in the normal human brain. Radiology 1991;181: 537–543.
27. Drayer B, Burger P, Hurwitz B, Dawson D, Cain J. Reduced signal intensity on MR images of thalamus and putamen in multiple sclerosis: increased iron content? AJR Am J Roentgenol 1987;149: 357–363.
28. McNeill A, Birchall D, Hayflick SJ, et al. T2* and FSE MRI distinguishes four subtypes of neurodegeneration with brain iron accumulation. Neurology 2008;70:1614–1619.
29. Gelman N, Gorell JM, Barker PB, et al. MR imaging of human brain at 3.0 T: preliminary report on transverse relaxation rates and relation to estimated iron content. Radiology 1999;210:759–767.
30. Gerlach M, Ben-Shachar D, Riederer P, Youdim MB. Altered brain metabolism of iron as a cause of neurodegenerative diseases? J Neurochem 1994;63:793–807.
31. Bartzokis G, Tishler TA, Lu PH, et al. Brain ferritin iron may influence age- and gender-related risks of neurodegeneration. Neurobiol Aging 2007;28:414–423.
32. Beaulieu C. The basis of anisotropic water diffusion in the nervous system—a technical review. NMR Biomed 2002;15:435–455 (Review).
33. Barnea-Goraly N, Eliez S, Hedeus M, et al. White matter tract alterations in fragile X syndrome: preliminary evidence from diffusion tensor imaging. Am J Med Genet B Neuropsychiatr Genet 2003;118:81–88.
34. Zaja-Milatovic S, Milatovic D, Schantz AM, et al. Dendritic degeneration in neostriatal medium spiny neurons in Parkinson disease. Neurology 2005;64:545–547.
35. Baquet ZC, Gorski JA, Jones KR. Early striatal dendrite deficits followed by neuron loss with advanced age in the absence of anterograde cortical brain-derived neurotrophic factor. J Neurosci 2004;24:4250–4258.
36. Wegner C, Esiri MM, Chance SA, Palace J, Matthews PM. Neocortical neuronal, synaptic, and glial loss in multiple sclerosis. Neurology 2006;67:960–967.
37. Wylezinska M, Cifelli A, Jezzard P, Palace J, Alecci M, Matthews PM. Thalamic neurodegeneration in relapsing-remitting multiple sclerosis. Neurology 2003;60:1949–1454.
38. Douaud G, Poupon C, Cointepas Y, Mangin JF, Gaura V, Golestani N. Diffusion tensor imaging (DTI) in Huntington's disease patients: analyses of fractional anisotropy (FA) maps and apparent diffusion coefficient (ADC) maps. In: Proceedings of the ISMRM Workshop on Methods for Quantitative Diffusion MRI of Human Brain, Lake Louise, Canada, 2005, p 23.
39. Hasan KM, Sankar A, Halphen C, et al. 2008. Quantitative diffusion tensor imaging and intellectual outcomes in spina bifida. J Neurosurg Pediatr 2008;2:75–82.
40. Ciccarelli O, Werring DJ, Wheeler-Kingshott CA, et al. Investigation of MS normal-appearing brain using diffusion tensor MRI with clinical correlations. Neurology 2001;56:926–933.